Characterization of Mo/Si mirror interface roughness for different Mo layer thickness using resonant diffuse EUV scattering

Anton Haase[a], Victor Soltwisch[a], Frank Scholze[a] and Stefan Braun[b]

[a]Physikalisch-Technische Bundesanstalt, Abbestr. 2-12, 10587 Berlin, Germany;
[b]Fraunhofer IWS, Winterbergstr. 28, 01277 Dresden, Germany

ABSTRACT

The throughput of extreme ultraviolet (EUV) lithography systems is presently strongly limited by the available radiant power at the wafer level. Besides increasing the power of EUV sources, also the quality of the optical elements plays a key role. With state of the art multilayer mirrors the main cause of diminished reflectance is surface and interface roughness as well as interface diffusion. Both properties lead to reduced specular reflectance while only the interface roughness causes diffuse scattering. EUV diffuse scatter thus allows to selectively assess the contribution of the interface roughness

The intensity distribution of diffusely scattered EUV radiation provides information on vertical and lateral correlations of the surface and interface roughness through the appearance of resonant diffuse scattering (RDS) sheets. The study of off-specular scattering thus serves as a natural tool for the investigation of the roughness of the interfaces. However, upon near-normal incidence impinging EUV radiation, dynamical scattering contributions from thickness oscillations (Kiessig fringes) lead to Bragg lines which intersect the RDS sheets. This causes strong resonant enhancement in the scatter cross section which we called "Kiessig-like peak" in analogy to the well known phenomenon of Bragg-like peaks appearing in hard X-ray grazing incidence measurement geometries. Thus for power spectral density studies of multilayer interface roughness, resonant dynamical scattering cannot be neglected. Theoretical simulations based on the distorted-wave Born approximation enable to separate dynamic features of the multilayer from roughness induced scattering. This allows to consistently determine an interface power spectral density (PSD). We have analyzed magnetron sputtered high-reflectance Mo/Si multilayer mirrors with different nominal molybdenum layer thicknesses from 1.7 nm to 3.05 nm crossing the Mo crystallization threshold.

Our off-specular scattering measurements at multilayer samples were conducted at the PTB-EUV radiometry beamline at the Metrology Light Source (MLS) in Berlin. The samples were produced by magnetron sputtering and pre-characterized by K_α X-ray reflectivity at Fraunhofer IWS, Dresden.

Keywords: Multilayer, scattering, roughness, diffusion

1. INTRODUCTION

With shrinking feature sizes in integrated circuits, the semiconductor industry is on the verge to implement a major switchover in the technological realization of optical lithography. While the current production systems operate at the UV wavelength of 193 nm, future EUV lithography systems will operate at 13.5 nm EUV wavelength. Alongside with the change in wavelength, the non-existence of low-absorbance transmissive optics in this spectral range enforces a switch from transmissive to reflective geometry. Multilayer optics are key elements for the ongoing development of future and present optical lithography systems.[1] Accompanying this, the available power at the wafer level is limiting the throughput and thus the efficiency of the lithography system. Apart from the source power, the gap between theoretical maximum reflectivity and experimentally measured reflectivity of the multilayer mirrors employed are the main reason for reduced performance throughout the array of optics. It is thus essential to gain fundamental understanding about the loss mechanisms involved. This applies even more

---

to possible future steps towards even shorter wavelengths, where the gap between theoretical and experimental peak reflectivity is larger.

Multilayer mirrors optimized for near-normal incidence reflectivity are composed out of stacks of two alternating materials with high optical contrast for the desired wavelength and low absorption.[2] High reflectivities are the result of contructive interference of radiation reflected at each interface of this artificial one-dimensional Bragg reflector. The Molybdenum/Silicon multilayer samples investigated here are optimized to reflect radiation of 13.5 nm for an incidence angle of 6 degrees from normal incidence. The main reason for loss of reflectivity is interdiffusion and roughness at the interfaces of this stack, leading to reduced optical contrast and thus reduced reflectivity. While interdiffusion merely causes a decline in peak reflectivity, roughness causes additional off-specular diffuse scattering. We investigate the diffuse scattering, which serves as a natural tool to explore the properties of roughness and interdiffusion at the interfaces for three samples. The samples differ in the thickness of the Molybdenum in each period. The nominal thickness values range from $d_{Mo} = 2.30$ nm to $d_{Mo} = 3.05$ nm, crossing the crystallization threshold of the Mo layer.

2. EXPERIMENTAL METHOD

The Physikalisch-Technische Bundesanstalt (PTB) operates two EUV beamlines, one at the electron storage ring BESSY II and a second at its own storage ring Metrology Light Source (MLS) for at-wavelength metrology.[3] All data presented here was measured at the EUVR beamline at the MLS. The end station is a large reflectometer shown in Fig. 1 with 2 m in chamber diameter capable of holding large samples, e.g. collector mirrors. These are large, strongly inward curved multilayer mirrors which can not be subjected to grazing incidence scattering experiments due to simple geometric limitations. The reflectometer is equipped with a goniometer and a movable detector arm with a 4.5 mm × 4.5 mm photo diode. Together with the accessible wavelength range between 5 nm and 50 nm of the SX100 monochromator, angle and energy resolved measurements of the diffuse scattering from Mo/Si multilayer mirrors optimized for 13.5 nm peak reflectivity are possible.
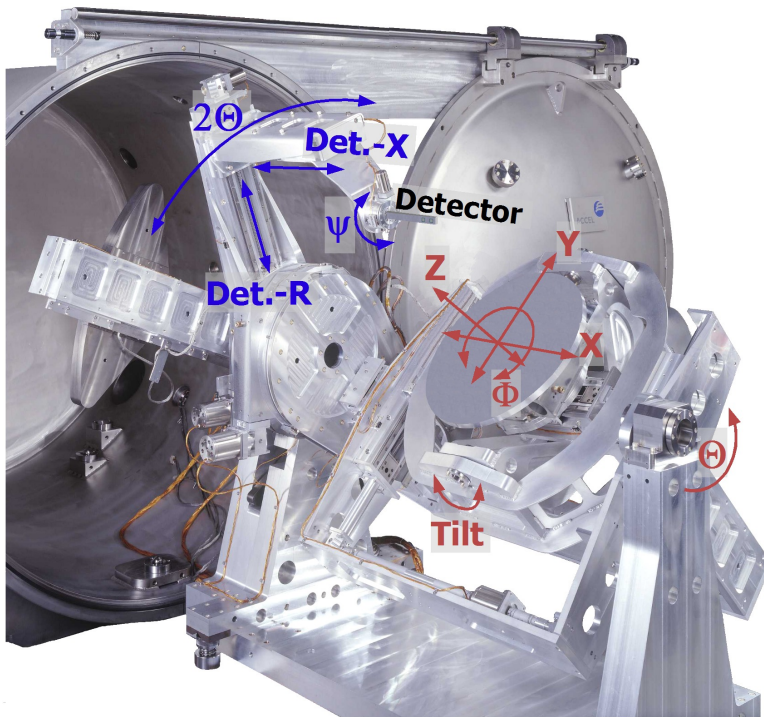

Figure 1: Reflectometer with goniometer and detector axes

Recording in-plane reciprocal space maps with detector movements in the scattering plane spanned by surface normal and incoming beam vector near normal incidence, requires performing angular as well as wavelength scans.

This measurement geometry is shown in Fig. 2(a). The reciprocal space is spanned by the reciprocal space vector components

$$q_x = \frac{2\pi}{\lambda}\big(\sin(\Theta) - \sin(\alpha_i)\big), \tag{1}$$

$$q_z = \frac{2\pi}{\lambda}\big(\cos(\Theta) + \cos(\alpha_i)\big), \tag{2}$$

where λ is the wavelength, α_i is the angle of incidence and Θ is the position of the detector with respect to the surface normal. The paths through reciprocal space depending on angular motion of either the detector or the sample, as well as a scan across several wavelengths is also shown in Fig. 2(b).
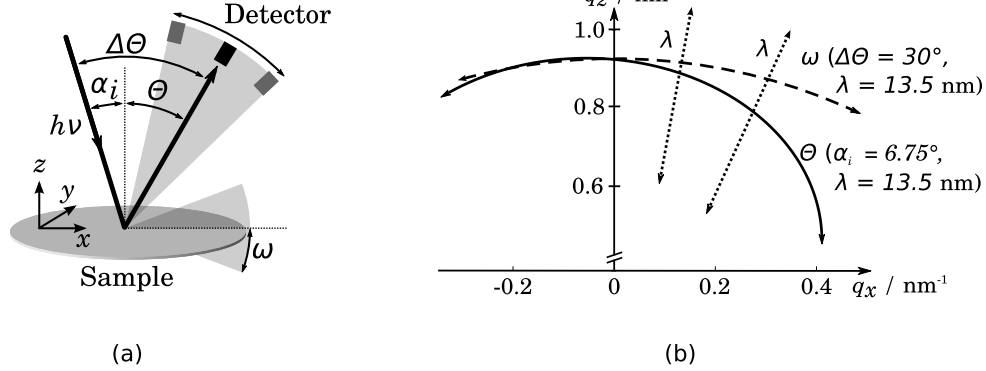

(a)   (b)

Figure 2: (a) Measurement geometry with sample and detector movement; (b) Paths through reciprocal space when moving the detector or rocking the sample, as well as scans across different wavelengths in dependence on the angular position

The pre-characterization applying grazing incidence reflectivity measurements of the samples using radiation from a copper K_α tube was conducted at the Fraunhofer IWS.

3. THEORETICAL BACKGROUND

We analyze the diffuse scattering maps on the basis of the distorted-wave Born approximation (DWBA).[4–8] The extraction of the mean power spectral density describing the statistical characteristics of the interfaces and their correlations is not straight forward. In the case of near-normal incidence scattering of EUV radiation from multilayer mirrors, dynamic effects cause enhancements in the off-specular scattering. Only the incorporation of multiple reflections and resonant enhancement due to thickness oscillations enables the consistent extraction of the PSD. A detailed description of the method can be found here[9] and will be described briefly in the following.

As a prerequisite for the application of the DWBA, the field intensities at the interfaces have to be calculated. This is done by applying a matrix formalism[10] to solve the wave equation for the modeled multilayer system exactly using the well known Fresnel coefficients $r_{id}^{(j)}$ and $t_{id}^{(j)}$ to evaluate the reflected and transmitted field amplitude at each interface i. The wavefield can then be decomposed into the part propagating towards the surface $E_r^{(j)}(z)$ and a part propagating towards the substrate $E_t^{(j)}(z)$ defined as,

$$E_t^{(j)}(z) = T_j e^{ik_z^{(j)}z}, \tag{3}$$

$$E_r^{(j)}(z) = R_j e^{-ik_z^{(j)}z}. \tag{4}$$

with $E_{id}^{(j)}(\mathbf{r}) = e^{i\mathbf{k}_\parallel \mathbf{r}_\parallel}(E_t^{(j)}(z) + E_r^{(j)}(z))$ being the full solution of the wave equation. The amplitudes of the two field components are then defined by T_j and R_j calculated by application of the matrix formalism.

The high quality of the multilayer requires to explicitly incorporate the reflected field intensities in the diffuse scattering computations at each interface in first order. Particularly the side fringes of the specular

reflectivity curve can resonantly enhance diffusely scattered light and cause strong maxima in the reciprocal space maps. Eq. 5 separates out the contributions of the multilayer from the actual contributions from the interface morphology $C(q_x)$ to the scattered intensity,

$$
\left(\frac{d\sigma}{d\Omega}\right) = \left[\frac{A\pi^2}{\lambda^4} \sum_{j=1}^{N} \sum_{i=1}^{N} (n_j^2 - n_{j+1}^2)^* (n_i^2 - n_{i+1}^2) \left((T_j^{(1)} + R_j^{(1)})^* (T_j^{(2)} + R_j^{(2)})^* \right. \right.
$$

$$
\left. \left. \times (T_i^{(1)} + R_i^{(1)})(T_i^{(2)} + R_i^{(2)}) \right) \exp\left(-iq_x \tan\beta(z_i - z_j) \right) c_\perp^{ij} \right] C(q_x). \tag{5}
$$

The contribution of the interfaces is contained within $C(q_x)$, which is the mean power spectral density (PSD)[6,7] of all interfaces. $C(q_x)$ is parameterized using a model[11] based on fractal surface and interface roughness as

$$
C(q_x) = \frac{4\pi H \sigma^2 \xi_\parallel^2}{(1 + |q_x|^2 \xi_\parallel^2)^{1+H}}, \tag{6}
$$

where σ is the root mean square roughness, $\xi_\parallel$ is the lateral correlation length and H is the Hurst factor describing the jaggedness of the interfaces. The vertical correlation of the interface morphology is described by the replication factor[12] $c_{ij}^\perp(q_x)$ in Eq. 5 with the vertical correlation length $\xi_\perp$ in dependency on the spacial frequency q_x,

$$
c_{ij}^\perp(q_x) = \exp\left(- \sum_{n=\min(i,j)}^{\max(i,j)-1} d_n q_x^2 / \xi_\perp \right). \tag{7}
$$

Finally, an angle $\beta \neq 0$ in Eq. 5 accounts for roughness correlation not parallel to the surface normal, e.g. due to non-parallel growth of the multilayer stack during deposition.

4. RESULTS AND DISCUSSION

As mentioned above, structural information about the layer stacking is mandatory for the analysis of the diffuse scattering. The structural data is obtained by measuring specular X-ray reflectivity (XRR) of the samples. This was performed at-wavelength in the EUV range as well as using an X-ray tube at the copper K_α line $E = 8048$ eV. The simultaneous analysis of both data sets allows a more reliable analysis of the structural properties.[13] The fit was conducted using a particle swarm optimizer (PSO) in order to rule out converging to local minima. The fitted curves for both measurements are shown exemplary for Sample 3 in Fig. 3. The layer thicknesses obtained this way are listed in Table 1. It should be noted here, that the specificity for the Molybdenum thickness is much larger, fitting the EUV curve than for the other elements due to the difference in electron density. In addition, the samples all have 50 periods. In case of lower Mo thicknesses saturation of the peak reflectance is thus not reached, since the radiation penetrates through the multilayer stack into the substrate. This reduces the maximum reflectivity possible by the amount of radiation absorbed in the substrate. It becomes apparent by comparing the EUV reflectivity measured for Sample 1 and Sample 3 shown in Fig. 4. Sample 1 shows a significantly smaller peak width without significantly improved peak reflectance. By fitting the 50-period four-layer model incorporating the diffusion barriers B_4C and C, as well as a 2 nm SiO_2 layer on top, we found very good agreement of the Molybdenum thickness with the nominal values.

Table 1: Fit results of the specular EUV and XRR curves

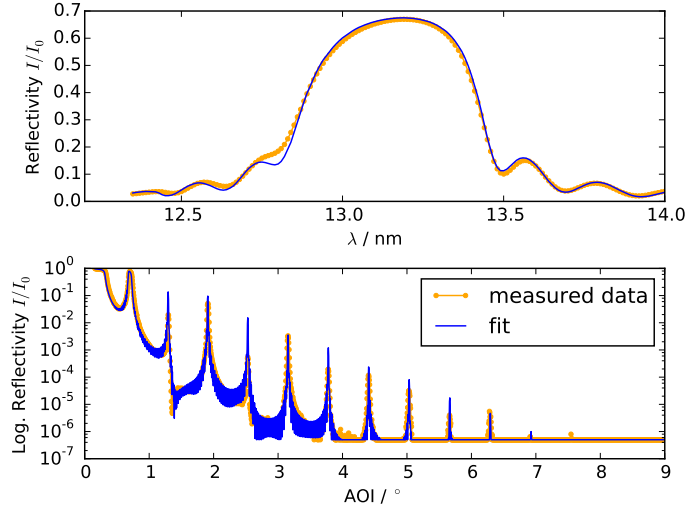| Sample by nom. Mo thickness	Si / nm	B4C / nm	Mo / nm	C / nm
Sample 1 (2.30 nm)	3.82	0.50	2.32	0.30
Sample 2 (2.60 nm)	3.73	0.50	2.68	0.07
Sample 3 (3.05 nm)	3.12	0.50	3.12	0.29

Figure 3: XRR and EUV reflectance measurements for Sample 3 with fit result. The EUV reflectance was recorded at an angle of incidence $\alpha_i = 15°$. The XRR curve was measured with a X-ray tube at the Cu K-α line at $E = 8048$ eV.

The samples were chosen in such a way, that the crystallization barrier of Molybdenum expected at thicknesses larger than approximately 2.30 nm, is crossed from one sample to the next. The specular reflectivity curves recorded at an angle of incidence $\alpha_i = 15°$ are shown in Fig. 4. Sample 1 with a fitted Mo thickness of $d_{Mo} = 2.32$ nm shows a higher reflectivity than Sample 2 with $d_{Mo} = 2.68$ nm, which is well above the crystallization barrier. We thus conclude that the Mo layer in Sample 1 is amorphous, where Sample 2 contains crystallized Mo. Sample 3 with a Mo thickness of $d_{Mo} = 3.12$ well above the crystallization threshold shows a reflectivity comparable to Sample 1.

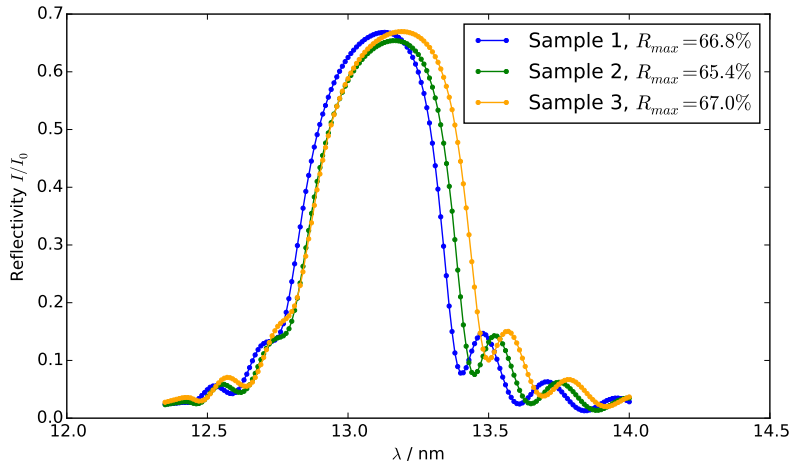Figure 4: EUV reflectance curves for Samples 1-3 measured at $\alpha_i = 15°$.

We performed diffuse scattering measurements for all three samples applying the method described in Sec. 3. The reciprocal space maps were recorded at an opening angle between incoming beam and detector of $\Delta\Theta = 30°$, while rocking the sample from $\alpha_i = 15°$ through $\alpha_i = 45°$. The results are shown together in Fig. 5. All samples show strong resonant diffuse scattering overlayed by dynamic Kiessig resonances indicating high degree of vertical

roughness correlation. In addition, a strong downward tilt can be observed in all three cases suggesting a non-orthogonal roughness correlation w.r.t. the surface. The total amount of scattered radiation is found to be strongest with Sample 2, while it is significantly lower for Samples 1 and 3. The model was fitted to cuts at regular angular positions by applying Eq. 5 and based on the structural properties listed in Table 1. The fitted
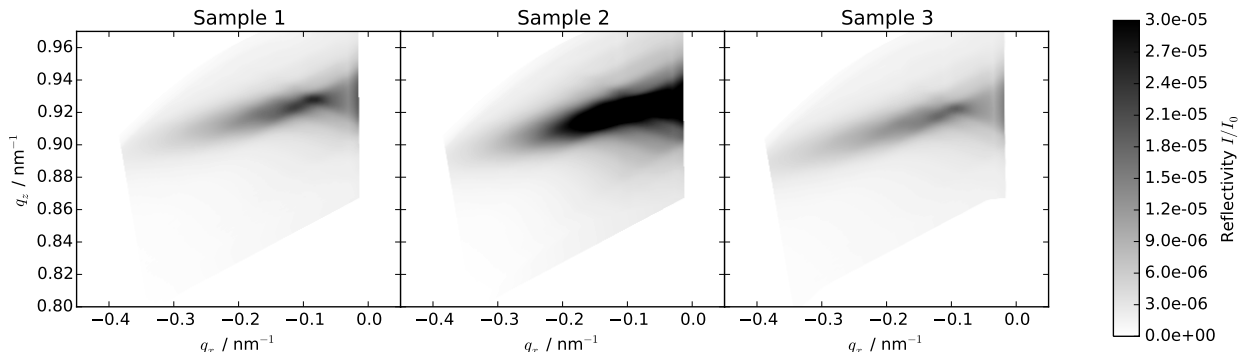

Figure 5: Reciprocal space maps of Samples 1-3 recorded with an opening angle $\Delta\Theta = 30°$ in the wavelength range from $\lambda = 12.4$ nm to $\lambda = 14.0$ nm.

power spectral densities (cf. Eq. 6) of all three samples are listed in Table 2. All samples show very high vertical

Table 2: Fit results for the reciprocal space maps.

Sample by nom. Mo thickness	σ_{rms} / nm	$\xi_{\parallel}$ / nm	$\xi_{\perp}$ / nm	H	β / °
Sample 1 (2.30 nm)	0.224	3.74	7.39	0.99	-4.26
Sample 2 (2.60 nm)	0.286	4.98	7.83	0.99	-4.38
Sample 3 (3.05 nm)	0.225	3.00	9.98	0.99	-4.89

roughness correlation. According to the model from Eq. 7, the vertical correlation length is dependent on the spacial frequency of the roughness. The fit results show full correlation through the whole stack of the multilayer with total thickness D up to approx. $q_x = -0.1$ nm^{-1}. At $q_x = 0.2$ nm^{-1} we still observe correlation lengths in the order of $D/2$. As mentioned above, in addition we observe a tilt of the associated Bragg sheet suggesting a non-orthogonal correlation of roughness vertically by the angle β listed in Table 2. The lateral correlation length $\xi_{\parallel}$ is comparable for Sample 1 and 3, while being significantly larger for Sample 2. Similarly the root mean square roughness σ is much larger for Sample 2 than for the other two samples. Together this shows that the appearance of crystallites in the Mo layer causes a strong increase in roughness at the interfaces. The strong vertical correlation leads to replication of this roughness through the stack. The larger lateral correlation lengths in this case suggests a strong increase in special frequencies from $q_x = 0.02$ nm^{-1} (lower limit of the measurement) to $q_x = 0.2$ nm^{-1} due to the crystallization. Additional deposition above the crystallization threshold, i.e. as seen for Sample 3, tends to restore the low roughness values found for Sample 1.

5. CONCLUSIONS

We present the characterization of Mo/Si multilayer mirrors with respect to the interface morphology applying off-specular diffuse scattering measurements. The analysis of the obtained reciprocal space maps requires explicit modeling of the structural properties of the multilayer to incorporate dynamic effects causing strong enhancement in the off specular scattering. We employ the distorted-wave Born approximation to separate the resonant enhancement caused by the multilayer from the effect of the interface morphology. The results show increased roughness for Mo layer thicknesses close to the thickness threshold for crystallization, especially for roughness frequencies $q_x < 0.2$ nm^{-1}. This additional roughness causes a diminished reflectivity. However, even thicker Mo layers aid in smoothing this roughness returning the reflectivity and diffuse scattering to values comparable to the Sample 1 below the threshold.

REFERENCES

1. Feigl, T., Yulin, S., Benoit, N., and Kaiser, N., "{EUV} multilayer optics," *Microelectronic Engineering* **83**(4–9), 703 – 706 (2006). Micro- and Nano-Engineering {MNE} 2005 Proceedings of the 31st International Conference on Micro- and Nano-Engineering.

2. Braun, S., Mai, H., Moss, M., Scholz, R., and Leson, A., "Mo/si multilayers with different barrier layers for applications as extreme ultraviolet mirrors," *Japanese journal of applied physics* **41**(part 1), 4074–4081 (2002).

3. Tümmler, J., Blume, H., Brandt, G., Eden, J., Meyer, B., Scherr, H., Scholz, F., Scholze, F., and Ulm, G., "Characterization of the ptb euv reflectometry facility for large euvl optical components," *Proc. SPIE* **5037**, 265–273 (2003).

4. Holý, V. and Baumbach, T., "Nonspecular x-ray reflection from rough multilayers," *Phys. Rev. B* **49**, 10668–10676 (Apr 1994).

5. Holý, V., Kuběna, J., Ohlídal, I., Lischka, K., and Plotz, W., "X-ray reflection from rough layered systems," *Phys. Rev. B* **47**, 15896–15903 (Jun 1993).

6. Sinha, S. K., Sirota, E. B., Garoff, S., and Stanley, H. B., "X-ray and neutron scattering from rough surfaces," *Phys. Rev. B* **38**, 2297–2311 (Aug 1988).

7. de Boer, D. K. G., "X-ray reflection and transmission by rough surfaces," *Phys. Rev. B* **51**, 5297–5305 (Feb 1995).

8. de Boer, D. K. G., "X-ray scattering and x-ray fluorescence from materials with rough interfaces," *Phys. Rev. B* **53**, 6048–6064 (Mar 1996).

9. Haase, A., Soltwisch, V., Laubis, C., and Scholze, F., "Role of dynamic effects in the characterization of multilayers by means of power spectral density," *Appl. Opt.* **53**, 3019–3027 (May 2014).

10. Born, M. and Wolf, E., [*Principles of Optics*], Cambridge University Press, 3 ed. (1965).

11. D.K.G. de Boer, A.J.G. Leenaers, and W.W. van den Hoogenhof, "Influence of roughness profile on reflectivity and angle-dependent x-ray fluorescence," *J. Phys. III France* **4**(9), 1559–1564 (1994).

12. Spiller, E., Stearns, D., and Krumrey, M., "Multilayer x-ray mirrors: Interfacial roughness, scattering, and image quality," *Journal of applied physics* **74**(1), 107–118 (1993).

13. Yakunin, S. N., Makhotkin, I. A., Nikolaev, K. V., van de Kruijs, R. W. E., Chuev, M. A., and Bijkerk, F., "Combined euv reflectance and x-ray reflectivity data analysis of periodic multilayer structures," *Opt. Express* **22**, 20076–20086 (Aug 2014).